International Journal of Nanomedicine Dovepress

Open Access Full Text Article ORIGINAL RESEARCH

Zinc-Based Nanoparticles, but Not Silicon-Based Nanoparticles, Accumulate in Mitochondria and Promote Cell Death in Liver Cancer Cells

Joana C Pieretti[1,2], Thaissa L Horne[1], Natalia García-Villasante[1], Amedea B Seabra[2], Jordi Muntané[1,3,4]

[1]Institute of Biomedicine of Seville (IBiS), Hospital University "Virgen del Rocío"/CSIC/University of Seville, Seville, Spain; [2]Center for Natural and Human Sciences, Federal University of ABC, Santo André, SP, Brazil; [3]Centro de Investigación Biomédica en red de Enfermedades Hepáticas y Digestivas (CIBEREHD), Madrid, Spain; [4]Department of Medical Physiology and Biophysics, University of Seville, Seville, Spain

Correspondence: Jordi Muntané, Instituto de Biomedicina de Sevilla (IBiS), IBiS/Hospital University "Virgen del Rocío/CSIC/University of Seville, Av. Manuel Siurot s/n, Seville, 41013, Spain, Tel +34-955923122, Fax +34-955923002, Email jmuntane-ibis@us.es

Introduction: Hepatocellular carcinoma (HCC) is the main hepatic primary malignancy. Patients with advanced HCC receiving the recommended therapies have a poor outcome. In different settings, nanotechnology has gained attraction as a potential alternative strategy for improving therapeutic effectiveness. Among several nanoparticles (NPs), inorganic NPs, such as zinc and silicon oxides (ZnO and SiO_2), are mainly chosen as drug nanocarriers, as both present great adsorption properties and biocompatibility.

Aim: The objective is to identify the molecular mechanisms underlying the proapoptotic effects of ZnO and SiO_2 NPs in differentiated hepatoblastoma cells (HepG2) and mesenchymal liver cancer cells (SNU449).

Methods: Dose-dependent induction of cell cytotoxicity by ZnO and SiO_2 NPs (5 to 50 µg/mL) was determined in HepG2 and SNU449 cells. NPs intracellular localization was assessed using transmission electron microscopy (TEM). Cell death was determined by trypan blue staining and caspase-3 and −8 activities. Cell respiration was determined using MitroStress assay (Seahorse, Agilent).

Results: ZnO NPs, but not SiO_2 NPs, reduced cell viability in HepG2 and SNU449. Interestingly, SNU449 appeared to be more susceptible than HepG2 to ZnO NPs (IC50 of 27.4 ± 1.4 µg/mL and 41.8 ± 0.4 µg/mL, respectively). SiO_2 NPs tended to be localized in lysosomes in both cell lines, while ZnO NPs demonstrated a random distribution with a high presence in mitochondria and related structures. As expected, SiO_2 NPs did not reduce cell survival and cell respiration, while ZnO NPs promoted cell death and decreased oxygen consumption rate. ZnO NPs mitochondrial accumulation was associated with increased apoptosis in HepG2, while necroapoptosis was mainly involved in ZnO-induced cell death in SNU449.

Conclusion: SiO_2 demonstrated no cytotoxic profile against liver cancer cells. ZnO NPs demonstrated to accumulate in mitochondria impacting cell respiration and cell death in liver cancer cells. ZnO induced apoptosis and necroptosis in HepG2 and SNU449, respectively.

Keywords: apoptosis, cell respiration, hepatocellular carcinoma, metastasis, mitochondrial dysfunction

Introduction

The incidence and mortality rates of cancer are on the rise globally, representing a significant challenge to life expectancy gains in this century.[1] Among various forms of cancer, hepatocellular carcinoma (HCC) is the sixth most prevalent neoplasm, responsible for 600,000 deaths annually. HCC is the primary malignant tumor of the liver, developing in the context of cirrhosis in 80–90% of cases. A number of risk factors have been identified that are associated with the development of HCC. These include hepatitis B (HBV) and C (HCV) viral infections, alcohol consumption, aflatoxin B1, metabolic-associated steatotic liver disease (MASLD), tobacco use, diabetes and congenital diseases. The stage of the disease and the most appropriate therapeutic recommendations for patients with HCC are identified according to the Barcelona Clinic Liver Cancer (BCLC) criteria, taking into account the number, size and vascular invasion, presence of extrahepatic tumors, liver

Received: 19 April 2024
Accepted: 28 August 2024
Published: 23 November 2024

function and status of the patient.[2] The most effective treatments (radiofrequency, resection, and orthotopic liver transplant or OLT) are recommended for patients in the early stages of the disease (BCLC 0-A) with one to three tumors measuring less than or equal to 3 cm, good liver function (Child-Pugh A-B), asymptomatic (Performance Status 0), and no vascular invasion or extrahepatic metastasis. The five-year survival rate for these patients is between 50 and 80%, with an overall mean survival period exceeding 60 months.[3] However, currently, only one-third of patients diagnosed with HCC fall within the 0-A BCLC stage. Transarterial chemoembolization (TACE) using microspheres charged with doxorubicin is the recommended course of treatment for patients at the intermediate stage (BCLC B), with an overall mean survival of 26 months.[3] Patients with unfavorable prognostic factors, including vascular invasion, extrahepatic metastasis, and/or deterioration of liver function (BCLC C), are classified as advanced stage cases. They are recommended to receive Atezolizumab +Bevacizumab, Durvalumab+Tremelimumab, Sorafenib, and Lenvatinib as first-line therapies.[4] The overall mean survival of patients in the advanced stage receiving these treatments ranges from 11 to 19.2 months.[5]

It should be noted that administration of Sorafenib is associated with a number of complications, including fatigue, diarrhea, skin irritation, hand-foot syndrome (characterized by redness, pain, inflammation, and blisters on the palms or soles), hypertension, bleeding, weight loss, infections, peripheral nerve sensory disorders, and laboratory abnormalities (hypophosphatemia, hyperamylasemia, lipase). These adverse side effects result from the drug's lack of cell specificity and water insolubility. This necessitates the administration of high doses to ensure an effective treatment, which, in most cases, results in the reduction or suspension of the treatment.[6] In light of these considerations, there is a growing interest in exploring alternative therapeutic options and drug nanovectorization as potential avenues for enhancing efficacy while minimizing adverse effects, particularly within the context of modern oncology. A number of nano- and microparticle-based approaches are currently in development with the objective of reducing the dosage of Sorafenib. These include liposomes,[7] polymeric nanoparticles,[8,9] mesoporous nanoparticles (NPs),[10–12] core–shell microcapsules,[13,14] liquid crystalline NPs,[15] solid lipid NPs,[16–19] and neutral amphiphilic cyclodextrin-based nanocomposites.[20]

Among the various types of nanoparticles that have already been developed and characterized, silicon oxide (SiO_2) NPs and zinc oxide (ZnO) NPs have been selected with great frequency as nanocarriers due to their high drug adsorption potential and biocompatibility. SiO_2 NPs have become a cornerstone of nanomedicine, with their first use as drug carriers in 2001.[21] SiO_2 NPs are a highly biocompatible and biodegradable material with a large surface area and high pore volume, offering significant advantages over other nanocarriers. They are ideal for drug loading, with the ability to accommodate a diverse range of drugs, including (i) hydrophobic; (ii) hydrophilic drugs; (iii) proteins, and (iv) genes.[22] A review of the literature reveals that controlled drug release, higher biocompatibility, and improved drug stability in the biological environment are all benefits of associating the drug molecule with Si-NPs, as opposed to leaving it free (ie, non-associated with Si-NPs).[23] Similar to SiO_2 NPs, Zn-NPs and, more specifically, zinc oxide (ZnO) NPs, stand out for their biosafety. They are one of the five oxides considered safe and approved by the FDA. They are used, for example, as antimicrobial agents and sunscreens.[24,25] In addition to the potential for carrying drugs, similar to that observed with SiO_2 NPs, ZnO NPs also demonstrate promising antitumor activity.[25] The antitumoral potential of ZnO NPs has already been demonstrated in the treatment of melanoma cells,[26] breast cancer cells,[26] prostate cancer cells, and also HCC, demonstrating promising potential in cancer therapy.[25]

Despite the increasing development of nanocarriers, there is still a lack of literature demonstrating the NPs' mechanism in different cell lineages. The aim of this study is to compare the mechanism and future drug delivery potential of each NPs in differentiated and poorly differentiated HCC cell lines. This is the first report to assess the mechanism of both Si- and Zn-NPs, two main chosen NPs as drug nanocarriers, in differentiated hepatoblastoma cells and metastatic liver cancer cells. Furthermore, the study evaluates the best application of each nanomaterial for direct liver cancer treatment or their use as vectors for tyrosine kinase inhibitor incorporation.

Material and Methods

Synthesis and Characterization of SiO_2 and ZnO NPs

SiO_2 NPs were synthesized by sol-gel method as previously demonstrated by our group.[27] Tetraethyl orthosilicate (131903, Sigma Aldrich, San Luis, USA) was diluted in water (1:10 v/v) and mixed with absolute ethanol/ammonium

hydroxide (LabSynth, Diadema, Brazil) (10:1 v/v), in a proportion of 1:2. The mixture was vigorously stirred for 2 h and an excess of ethanol was added to stop the reaction. The obtained SiO_2 NPs were isolated by centrifugation, washed with ultrapure water, and dried at 60°C overnight. ZnO NPs were synthesized by the hydrothermal method adapted by our group.[28] Sodium hydroxide (1 mol/L) (LabSynth) was slowly added to an aqueous solution of zinc acetate dihydrate (10 mmol/L) (Z0625, Sigma-Aldrich, St Louis, USA) under constant stirring. The final suspension was transferred to an autoclave and incubated at 170°C for 10 hours. The resulting material was washed with absolute ethanol and deionized water and dried in an oven at 60°C for 2 hours. SiO_2 NPs and ZnO NPs were characterized by various techniques such as transmission electron microscopy (TEM, Carl Zeiss 120, Zeiss International, Oberkochen, Germany), X-ray diffraction (XRD, Stoe®, Darmstadt, Germany), Fourier transform infrared spectroscopy (FTIR, PerkinElmer, Waltham, MA, USA), dynamic light scattering (DLS) and electrophoretic mobility (Zetasizer nanoseries, Malvern Instruments, UK) to confirm their morphology, size and crystalline structure.

Cell Culture

Experimental procedures were carried out using a HepG2 cell line (Ref. HB-8065™, ATCC-LGC Standards, S.L.U., Barcelona, Spain), and SNU449 cell line (CRL-2234, ATCC/LGC Standards). Both cells were cultured in MEM with Earle's salts with L-glutamine with non-essential amino acids (Ref. 11140035, Gibco, ThermoFisher Scientific, Waltham, USA), penicillin-streptomycin solution (100 U/mL-100 µg/mL) (Ref. 15640055, Gibco), sodium pyruvate (1 mmol/L) (Ref. 11360070, Gibco), and 10% fetal bovine serum (FBS) (F7524, Sigma-Aldrich), in a humidified incubator with 5% CO_2, at 37°C. Cells were plated at 100,000 cells cm^2 and allowed to stabilize for 24 hours prior to treatment. Stock SiO_2 and ZnO NPs (2 mg/mL) were sonicated and diluted according to each concentration evaluated.

Cell Viability Assay

Trypan blue staining was used to assess cell viability.[29] Cells were treated with a wide range of SiO_2 or ZnO NPs (5, 15, 20, 30, 40 and 50 µg/mL). After 24 hours, cells were harvested and stained with trypan blue. The percentage of blue relative to the total number of cells was used as a marker of reduced cell viability. A similar procedure was used to evaluate cell viability in the presence of necroptosis and ferroptosis inhibitors. Necrostatin-1 (50 µmol/L) (480065, Sigma Aldrich) and ferrostatin-1 (10 µmol/L) (SML0583, Sigma Aldrich) were administered 30 min before NPs.[30,31] The experiment was then performed as described above.

SiO_2 and ZnO Cellular Localization

HepG2 and SNU449 cells treated with either SiO_2 or ZnO NPs (15 µg/mL) were analyzed by TEM (Zeiss Libra 120, Zeiss International) to investigate the localization of NPs in HCC cells. After 24 hours of treatment, cells were harvested and fixed with glutaraldehyde (2.5%) for 1 hour at 4°C. After removal of the fixative, cells were washed several times with cacodylate 0.1 mol/L and postfixed with osmium (1%) for 1 hour at 4°C.[32] The samples were washed with distilled water and uranyl (2%) was added. Finally, the samples were dehydrated and immersed in resin which was polymerized at 60°C.[32] The resin was cut into 70 nm slices, which were placed on TEM grids for posterior visualization.

Activation of Endocytic Pathways

The involvement of endocytic pathways in NPs uptake was assessed by the fluorescence of FM1-43 dye. Cells were plated on glass slides pretreated with poly-lysine/collagen (1:1). Cells were treated with ZnO or SiO_2 NPs (15 µg/mL) for 10 minutes in the absence of a dynamin inhibitor, dynasore monohydrate (D7693, Sigma Aldrich), followed by the addition of FM1-43 (T3163, Invitrogen). Rapamycin 200 nmol/L (37094, Sigma Aldrich) was used as a positive control.[33] Cells were visualized within 10 min after the dye addition using a confocal microscope Nikon A1R+ (Nikon, Tokyo, Japan), coupled with an argon laser for excitation at 473 nm and emission at 579 nm. Images were obtained using 40x lens, a pinhole of 1.0, and an argonium laser with a potency of 3.5 and a HV(G) of 65 (Ex 488/Em 570–620).

Caspase 3 and 8 Activities

Caspase-3- and caspase-8-associated activities were determined using Caspase-Glo®-3 and −8 assay systems (G8091 and G8200, respectively, Promega, Madison, USA) in HepG2 and SNU449 cells under treatment with SiO_2 or ZnO NPs (15, 20, 25, and 30 µg/mL) for 24 hours.[29] Cell lysate (20 µg protein in 20 µL) was incubated with 20 µL of commercial substrate for 1 hour at room temperature in the dark. Chemiluminescence was measured using an Infinite 200 PRO microplate reader (TECAN, Männedorf, Switzerland). Data were analyzed and expressed as percentage of untreated cells (control).

Cellular Respiration

Mitochondrial respiration or oxygen consumption rate (OCR) was assessed using the Cell MitoStress Test Kit (Ref. 103010–100, Agilent Technologies, Santa Clara, California USA) in the XF Pro Analyzer (Agilent Technologies).[34] Cells were plated on Seahorse XFe96/XF Pro cell culture microplates. Cell respiration was determined in SiO_2 or ZnO treated HepG2 and SNU449 cells. The protocol consisted of loading the sensor cartridge ports with 1 µmol/L oligomycin, 0.5 µmol/L FCCP, and 0.5 µmol/L rotenone/antimycin A. The assay medium consisted of basal medium (pH 7.4) supplemented with 1 mmol/L sodium pyruvate, 2 mmol/L glutamine, 10 mmol/L glucose.

Statistical Analysis

Data are expressed as mean ± standard error of the mean (SEM) from three to five independent experiments. Statistical analyses were performed using GraphPad Prism 8.0 software. Statistical significance was determined by analysis of variance (ANOVA) followed by Tukey's or Sidak's post-test, as described in the figure legends. The significance level was set at *p≤0.05, **p≤0.01, ***p≤0.001, and ****p≤0.0001.

Results

Synthesis and Characterization of SiO_2 and ZnO NPs

SiO_2 and ZnO NPs were successfully synthesized by sol-gel and hydrothermal synthesis, respectively, as shown in Figure 1. SiO_2 NPs showed a spherical morphology, with a solid size of 158 ± 20 nm and a hydrodynamic size of 155 ±

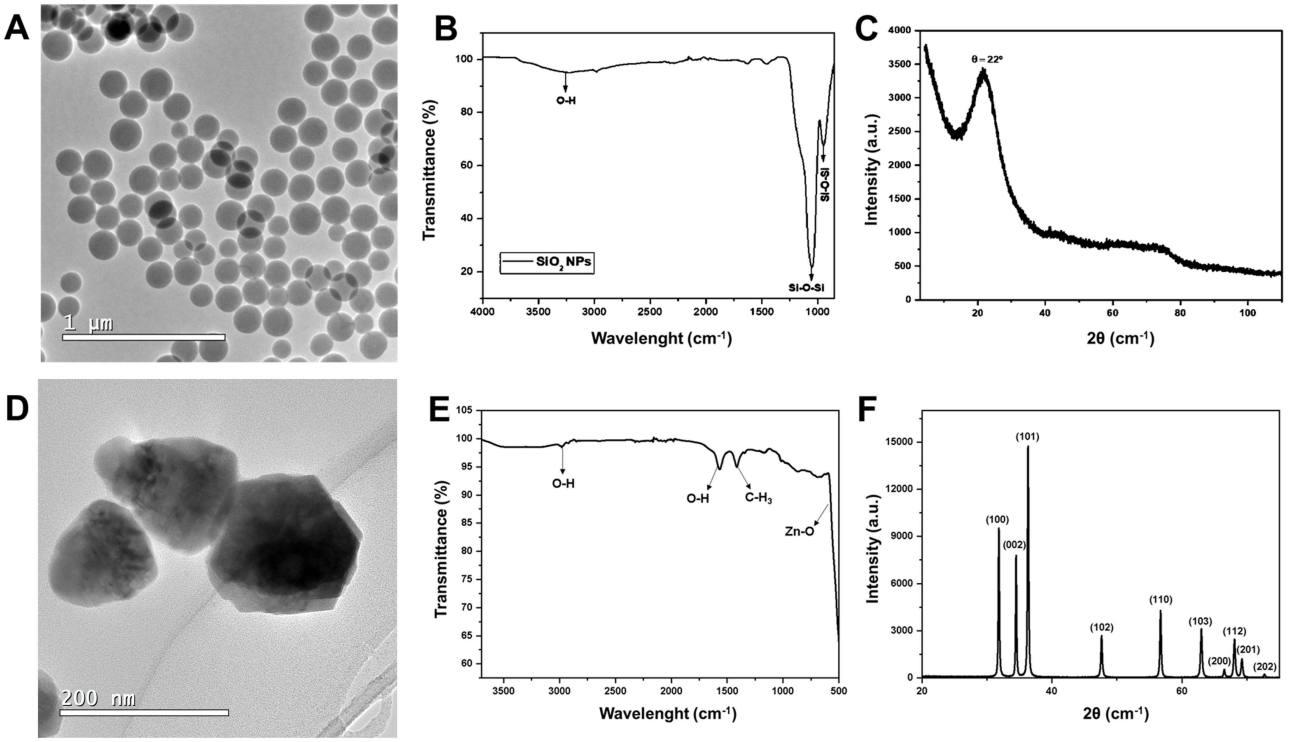

Figure 1 Physicochemical characterization of SiO_2 and ZnO NPs, showing transmission electron micrographs (**A** and **D**), FTIR spectra (**B** and **E**), and XRD diffractogram (**C** and **F**) of SiO2 NPs and ZnO NPs, respectively.

12.3 nm (% number), a polydispersity index (PDI) of 0.144 ± 0.044, and a zeta potential of −27.3 ± 0.5 mV. ZnO NPs showed a nanoplate morphology with a mean solid size of 89.5 ± 18.9 nm and a hydrodynamic size of 140.8 ± 17.3 nm, with a negative zeta potential of −20.57 ± 7.41 mV and a PDI of 0.23 ± 0.04. In addition, the hydrodynamic stability of both NPs was evaluated in phosphate buffer solution (PBS) or culture medium containing 10% FBS (Figure S1). For SiO_2 NPs, the hydrodynamic size was increased by 26% in PBS and decreased by 21% in culture medium containing 10% FBS, indicating a slight tendency of aggregation in the salt solution and a higher stability in the serum-containing medium. For ZnO NPs, a decrease of 13% was observed in PBS, while an increase of 19% was observed in culture medium containing 10% FBS. Overall, both NPs showed high stability in all the media evaluated.

The structure of both NPs was also confirmed by FTIR and XRD analysis. The FTIR spectra of SiO_2 NPs are shown in Figure 1B, which shows a characteristic stretching peak at 3413.68 cm^{-1}, corresponding to O-H stretching, and the bands related to asymmetric (1078 cm^{-1}) and symmetric (950 cm^{-1}) stretching of Si-O-Si.[35] The XRD diffractogram of SiO_2 NPs (Figure 1C) shows a characteristic peak at 2θ = 21°, corresponding to the amorphous silica structure.[36]

The FTIR spectrum of ZnO NPs is shown in Figure 1E. Characteristic and fundamental stretching bands were observed in the region of 2981 cm^{-1} and 1566 cm^{-1}, which correspond to the stretching of the -OH functional group,

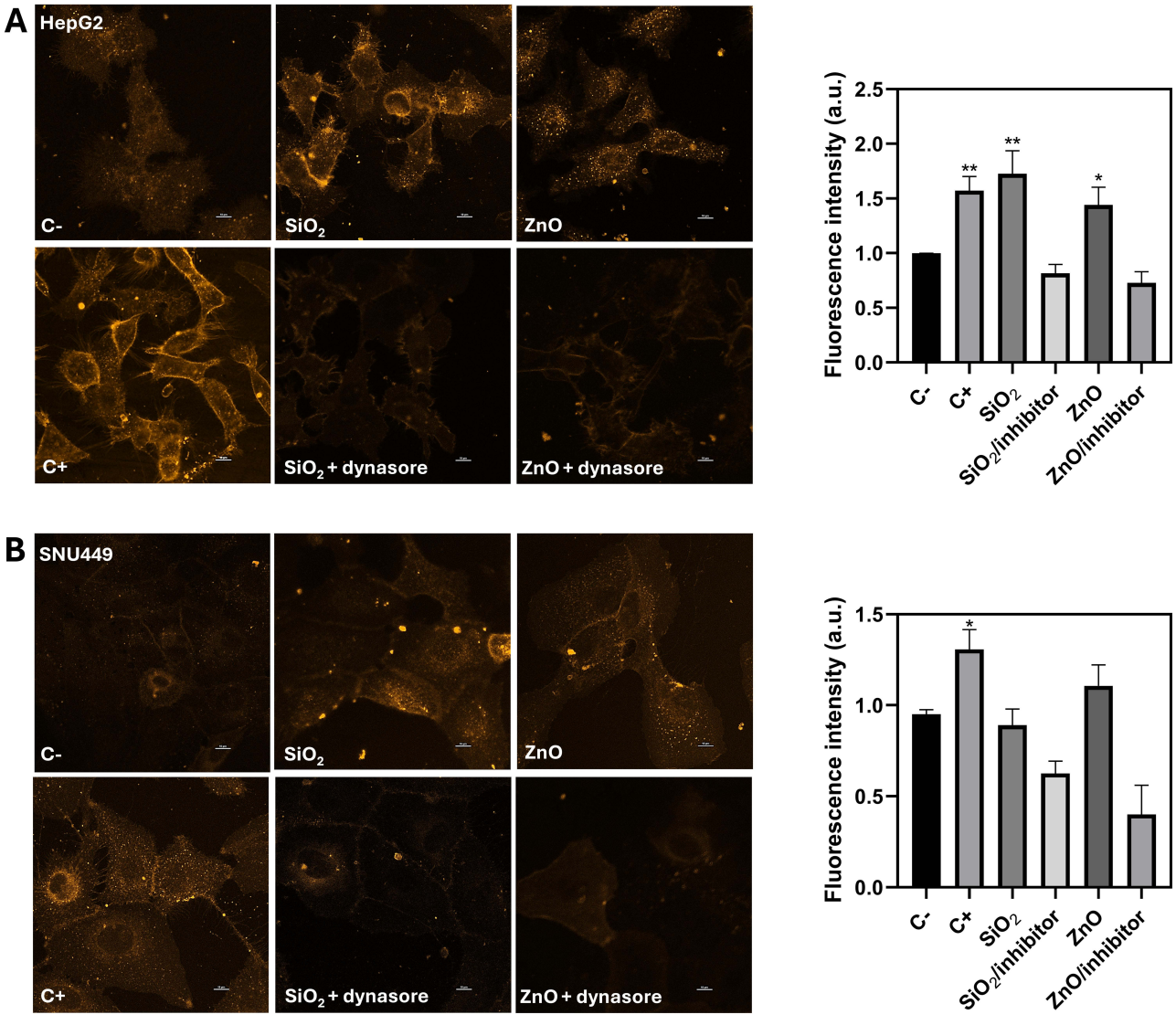

Figure 2 Endosomal incorporation of SiO_2 or ZnO (15 μg/mL) in HepG2 (**A**) and SNU449 (**B**) cells. The administration of rapamycin (200 nM) was used as a positive Control (C+). Inhibition of the endocytic pathway was performed with dynasore (80 μM). Data are expressed as the mean ± SEM of 5 independent experiments. **p≤0.01 and *p≤0.05.

while the bands at 1414 cm^{-1} and 688 cm^{-1} correspond, respectively, to -CH_3 absorption stretches and metal-oxygen (Zn-O) vibration mode in ZnO NPs.[37] Figure 1F shows the XRD analysis of ZnO NPs, indicating peaks at 2θ: 31.8°, 34.5°, 36.3°, 47.6°, 56.6°, 62.9°, 66.4°, 67.9°, 69.2° and 77.0°, which correspond respectively to the planes (100), (002), (101), (102), (110), (103), (200), (112), (201) and (202), confirming a hexagonal crystal geometry according to JCPSD card no. 01–007-2551.[38]

Incorporation of NPs in Liver Cancer Cells

NPs can be incorporated into cells by endocytosis or by non-endocytic mechanisms such as passive diffusion, pore formation, electroporation or microinjection.[39–41] We investigated the role of NPs-dependent endocytosis in a well-differentiated cell line (HepG2) and in a poorly differentiated cell line (SNU449). The FM1-43 probe was used to assess the involvement of the endocytic pathway during NPs uptake by cells.[42] Figure 2 shows the images of HepG2 (Panel A) and SNU449 (Panel B) cells stained with FM1-43, treated with either ZnO NPs or SiO_2 NPs, in the presence or absence of dynasore. Although the endocytic pathway appeared to be actively involved in NPs uptake based on the dynasore effect, the intensity of FM1-43 staining in HepG2 appeared to be more pronounced than that of SNU449 in the presence of ZnO NPs or SiO_2 NPs (Figure 2A and B).

SiO_2 and ZnO Cellular Localization

Intracellular accumulation of SiO_2 and ZnO NPs was determined by TEM in HepG2 and SNU449 cells. Control HepG2 and SNU449 are shown in Figure 3A and F, respectively. SiO_2 NPs accumulated in lysosome-like structures in both HepG2 (Figure 3B and C) and SNU449 cells (Figure 3G and H). ZnO NPs were mainly located in mitochondria in HepG2 cells (Figure 3D and E), while ZnO NPs were widely distributed in endoplasmic reticulum-like structures, cytoplasm, and finally in mitochondria and nuclei in SNU449 cells (Figure 3I and J).

Measurement of Cell Death Induced by SiO_2 or ZnO NPs

Cell death was determined by trypan blue exclusion (Figure 4, panel A), caspase-3 and −8 activities (Figure 4, panel B) in SiO_2- and ZnO-treated HepG2 and SNU449 cells after 24 hours. ZnO NPs induced a concentration-dependent cell membrane alteration in HepG2 and SNU449 cells. Interestingly, SNU449 appeared to be more sensitive to the effect of ZnO NPs than HepG2 with a significant decrease in cell viability at 20 µg/mL vs 50 µg/mL, respectively. The higher sensitivity of SNU449

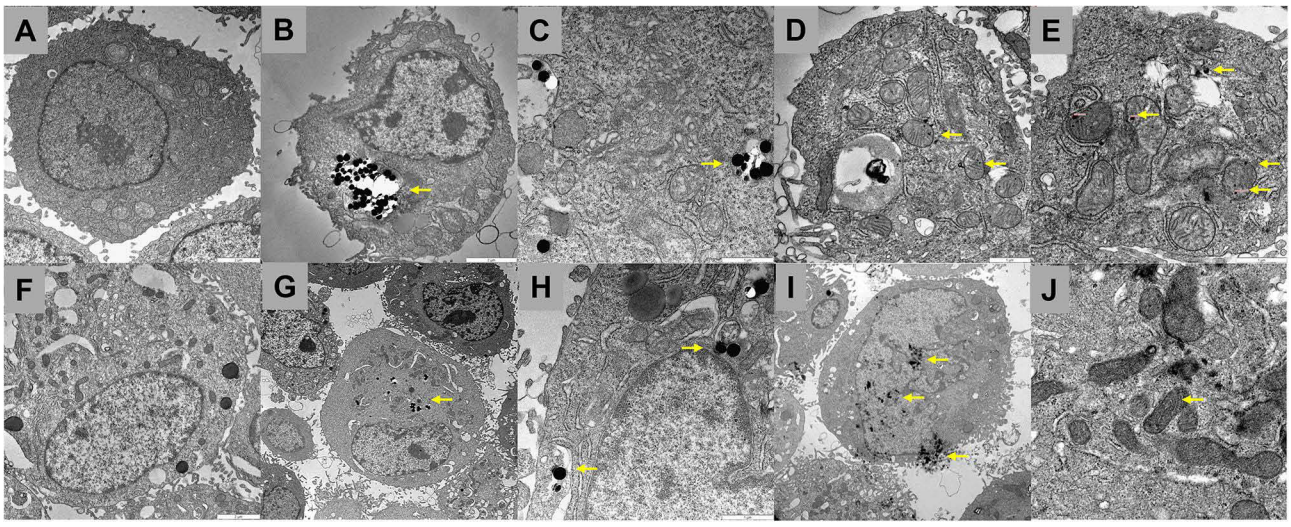

Figure 3 Transmission electron micrographs of (**A**) HepG2 control cells (2500x of magnification); (**B**) and (**C**) HepG2 cells treated with SiO_2 NPs (1600x and 6300x of magnification, respectively); (**D**) and (**E**) HepG2 cells treated with ZnO NPs (1600x and 6300x of magnification, respectively); (**F**) SNU449 control cells (2500x of magnification); (**G**) and (**H**) SNU449 cells treated with SiO_2 NPs (1600x and 6300x of magnification, respectively); (**I**) and (**J**) SNU449 cells treated with ZnO NPs (1600x and 6300x of magnification, respectively). Yellow arrows indicate the localization of SiO_2 NPs or ZnO NPs, inside HepG2 or SNU449 cells.

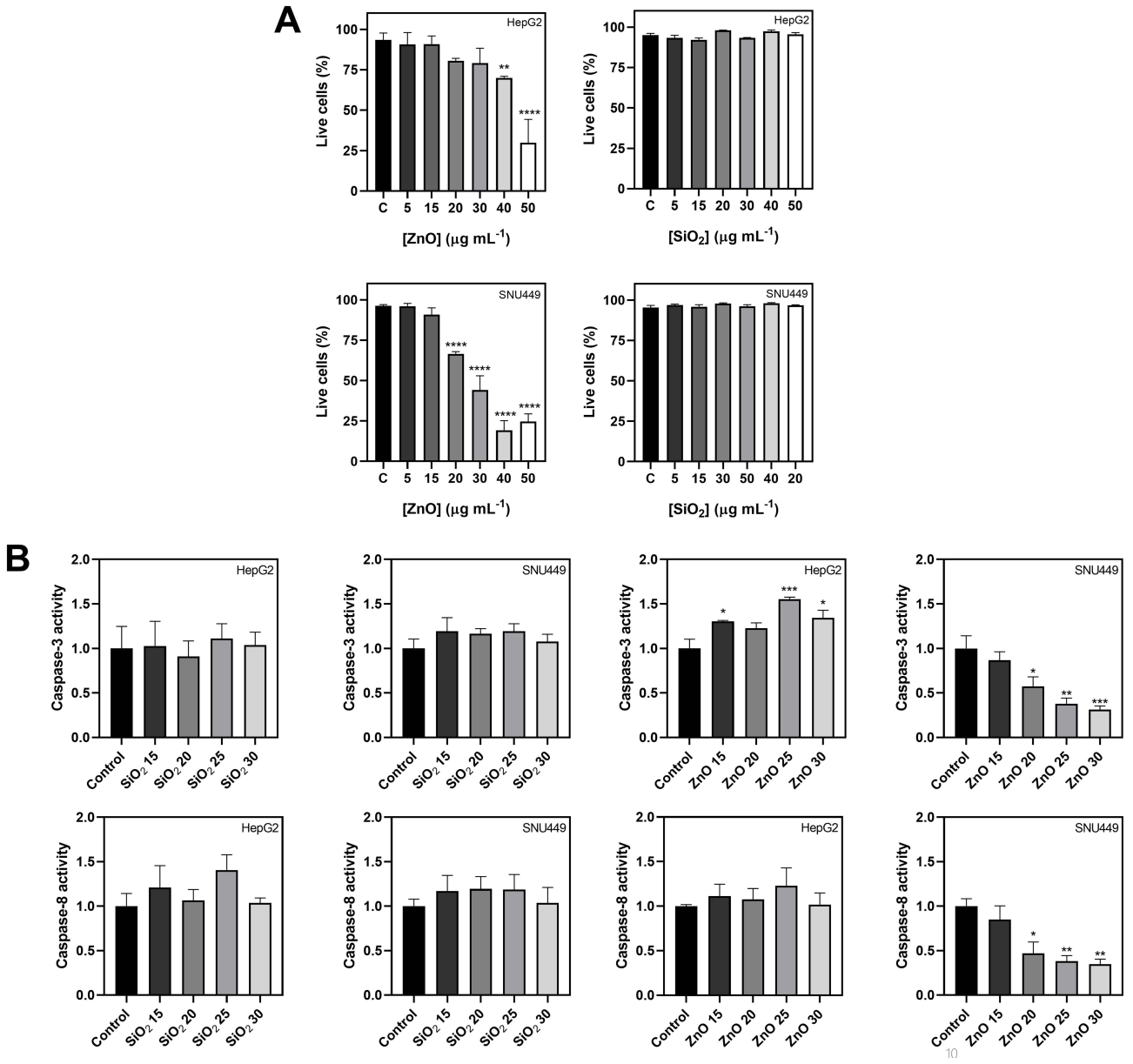

Figure 4 Cell viability of HepG2 and SNU449 cells treated with SiO_2 or ZnO NPs (5–50 μg/mL) for 24 h (**A**). Caspase-3 and −8 activities of HepG2 and SNU449 cells treated with SiO_2 or ZnO NPs (15, 20, 25 and 20 μg/mL) for 24 h (**B**). Data are expressed as the mean ± SEM of 3 independent experiments. ****$p \leq 0.0001$, ***$p \leq 0.001$, **$p \leq 0.01$ and *$p \leq 0.05$.

cells vs HepG2 cells to ZnO NPs was associated with a lower IC50 in SNU449 (27.4 ± 1.4 μg/mL vs 41.8 ± 0.4 μg/mL). In marked contrast, SiO_2 NPs did not affect cell viability in either HepG2 or SNU449 cells at any concentration tested.

Caspase-3 and −8 activities were used as a marker of apoptosis. Caspase-3 and −8 were not altered in SiO_2-treated HepG2 and SNU449 (left panel). ZnO NPs significantly increased caspase-3, but not caspase-8, in HepG2 (right panel). Interestingly, ZnO NPs reduced caspase-3 and caspase-8 in SNU449 cells in a dose-dependent manner. This different profile suggests different cell death patterns induced by ZnO NPs in HepG2 and SNU449.[43,44]

The involvement of ferroptosis and necroptosis in ZnO (50 μg/mL) NPs-induced cell death in HepG2 and SNU449 was determined using inhibitors such as ferrostatin-1 (10 mm) and necrostatin-1 (50 mm), respectively (Figure 5). Inhibition of ferroptosis and necroptosis did not alter the reduction in cell viability induced by ZnO NPs in HepG2 cells (Figure 5A and B). In contrast, although ferrostatin-1 did not alter the ZnO NPs-dependent reduction of cell viability,

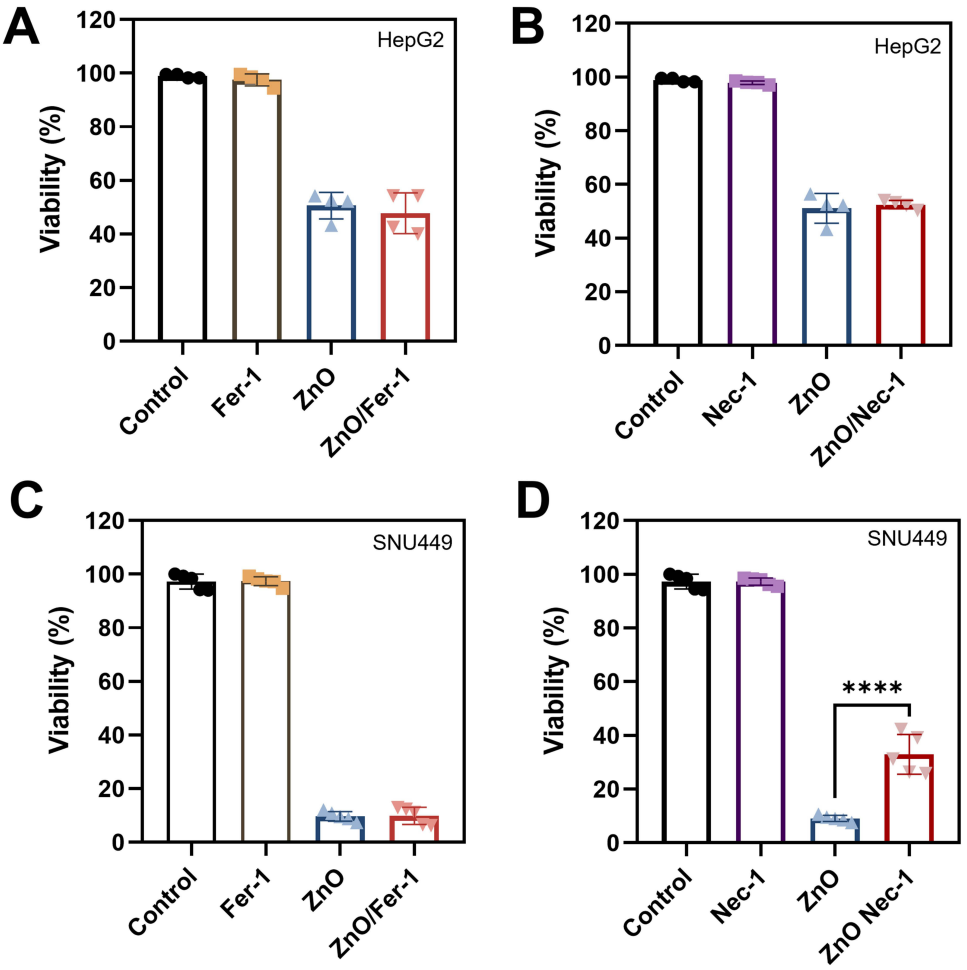

Figure 5 Effect of ferrostatin-1 (10 mm) and necrostatin-1 (50 mm) in the reduction of cell viability induced by ZnO NPs (50 µg/mL) in HepG2 (**A** and **B**, respectively) and SNU449 (**C** and **D**, respectively). Data are expressed as mean ± SEM from 3 independent experiments. ****$p \leq 0.0001$.

necrostatin-1 significantly restored cell viability from 9% to 33% in SNU449, suggesting that the necroptosis pathway might be involved (Figure 5C and D).

Cellular Respiration

We evaluated the alteration of mitochondrial respiration by NPs in HepG2 (Figure 6A) and SNU449 (Figure 6B) cells. SiO_2 NPs did not affect OCR (Figure 6A and B) and basal cell respiration (Figure 6C and D) in HepG2 and SNU449 cells, respectively. However, ZnO NPs reduced OCR in HepG2 cells even at non-cytotoxic doses. ZnO NPs drastically downregulated OCR (Figure 6A and B) and basal cell respiration (Figure 6C and D) in both cell lines.

Discussion

HCC is the most common form of primary liver cancer and is recognized as the fourth leading cause of cancer-related death worldwide, accounting for more than one million deaths annually by 2030.[45] In addition, only one-third of HCC patients are diagnosed in the early stages and are eligible for curative treatment; the remainder are in the intermediate/advanced stages with poor prognosis and a 5-year survival rate of less than 10%.[2] In this work, we aimed to determine the uptake, cellular distribution and cell death induced by SiO_2 and ZnO NPs in liver cancer cells at early and advanced stages of cell dedifferentiation (HepG2 and SNU449, respectively). HepG2 was derived from a well-differentiated liver tumor of a 15-year-old Caucasian American male and SNU449 was derived from a poorly differentiated, HBV-positive 52-year-old Korean male. Both cell lines are used as a reference of early and advanced liver cancer cells and represent

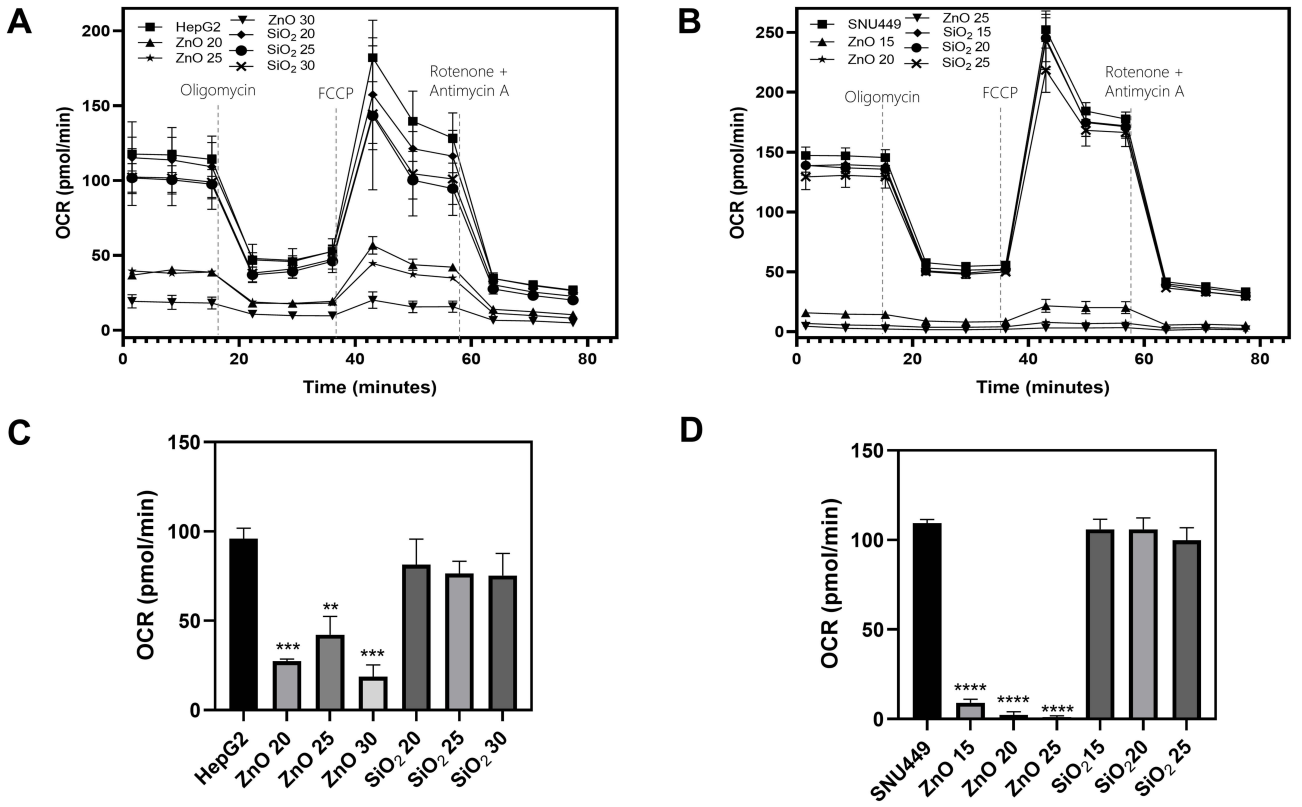

Figure 6 Alteration of oxygen consumption rate (OCR) (**A** and **B**) and basal cell respiration (**C** and **D**) by SiO_2 or ZnO NPs (0–30 μg/mL) for 24 h in cultured HepG2 and SNU449 cells, respectively. Data are expressed as the mean ± SEM of 4 independent experiments. ****$p \leq 0.0001$, ***$p \leq 0.001$ and **$p \leq 0.01$.

a suitable cell model to evaluate the efficacy of the NPs being studied.[46] SNU449 showed typical characteristics of mesenchymal cells with a lower response to Sorafenib than HepG2.[29] SiO_2 and ZnO NPs have been extensively studied in the field of nanomedicine. They have already been reported as promising nanocarriers for Sorafenib.[47] In addition, both NPs have already demonstrated an optimal range of biocompatibility.[22,28] The study sheds light on the molecular mechanisms of SiO_2 and ZnO NPs to incorporate and ultimately induce cell death in liver cancer cells. These features are relevant for the design of future NPs-based therapies.

Our results demonstrated that SiO_2 and ZnO NPs were able to be taken up by HepG2 and SNU449 cells via endocytic pathways, which appeared to be more active in the more differentiated cell line. This differential functionality of the endocytic pathway between HepG2 and SNU449 may be relevant to the increased efficacy of NPs in inducing cell death in SNU449 than in HepG2, considering that endocytosis fulfills several critical cellular functions, the effective degradation pathway being one of those that may be relevant in the present setting.[48] Furthermore, we observed that SiO_2 NPs accumulated in lysosomal-like cell compartments without any sign of cell death. In contrast, ZnO NPs were located in the mitochondrial compartment in HepG2 and were randomly distributed in the cytoplasm, endoplasmic reticulum-like structures, nucleus, and finally in the mitochondria in SNU449 cells. This differential distribution of ZnO NPs versus SiO_2 NPs was associated with increased caspase-3 and decreased OCR in HepG2. Interestingly, the wide intracellular distribution of ZnO NPs in SNU449 was associated with decreased caspase-3 and −8 activities, drastic downregulation of OCR, and identification of increased necrotic features such as increased trypan blue staining. The use of necrostatin-1 and ferrostatin-1 highlighted the importance of necroptosis in ZnO NPs-induced cell death in SNU449.

In agreement with our study, Sahu et al[49] have shown that ZnO exerts more potent concentration-dependent cytotoxicity than SiO_2 NPs in human lung epithelial cells (L-132) and human monocytes (THP-1). However, when the size of NPs was considered, it was observed that nano NPs tend to exert more potent cytotoxicity in L-132 and THP-1, especially in the presence of SiO_2.[49] The reduction of THP-1 survival rates by ZnO NPs was associated with the reduction of cell $\Delta\psi m$ and ATP levels and the generation of reactive oxygen species.[50] Our study showed that ZnO NPs

accumulated in the mitochondrial fraction, which may play a relevant role in mitochondrial dysfunction and reduced OCR induced by NPs.

These results indicate a promising use of both NPs against liver cancer cells, suggesting that each should be used differently. While SiO_2 NPs show great potential to carry drugs with low cytotoxicity, accumulating mainly in lysosomes, ZnO NPs could be used in advanced stages of the disease, even potentialized by combining a specific drug considering the mitochondrial target. We hope that with our results and future work in this field, antitumor treatments will be more personalized for an effective treatment with minimal side effects.

Conclusion

Although NPs demonstrated potential to be used as drug nanocarriers for future cancer treatments, the use of ZnO NPs exerted an additional cytotoxicity effect in liver cancer cells. The differential trafficking efficacy of differentiated versus metastatic liver cancer cells may influence the increased efficacy of ZnO NPs in SNU449 than HepG2 cells. ZnO NPs induced apoptotic cell death in HepG2, while necroptosis appeared to be associated with SNU449 cell death. Furthermore, the direct modification of mitochondrial function by ZnO NPs is highly relevant in the context of oncology. In fact, the antitumor properties of tyrosine kinase inhibitors are largely related to profound mitochondrial dysfunction.[29,51]

Abbreviations

BCLC, Barcelona-Clinic Liver Cancer; DLS, Dynamic light scattering; FTIR, Fourier transform infrared spectroscopy; HBV Hepatitis B virus; HCV, Hepatitis C virus; HCC, Hepatocellular carcinoma; MASLD, Metabolic-associated steatotic liver disease; NPs, Nanoparticles; OCR, Oxygen consumption rate; PDI, Polydispersity index; TACE, Transarterial chemoembolization; TEM, Transmission electron microscopy.

Acknowledgments

This study was funded by the Instituto de Salud Carlos III (ISCiii) (PI19/01266 and PI22/00857), Consejería de Salud y Familias (Junta de Andalucía) (PI-0216-2020 and PIP-0215-2020), São Paulo Research Foundation (Fapesp) (grant numbers: 2022/14645-2, ABS; 2021/12705-5, JCP; and 2020/03646-2, (JCP), and CNPq (313117/2019−5). This study was financed in part by the Coordenação de Aperfeiçoamento de Pessoal de Nível Superior - Brasil (CAPES) − Finance Code 001 (88881.711920/2022−01). We thank the Biomedical Research Network Center for Liver and Digestive Diseases (CIBERehd) founded by the ISCIII and co-financed by European Regional Development Fund "A way to achieve Europe" ERDF for their financial support.

Disclosure

The authors report no conflicts of interest in this work.

References

1. Chhikara BS, Parang K. Global Cancer Statistics 2022: the trends projection analysis. *Chem Biol Letters*. 2023;10(1):451.
2. European Association for the Study of the Liver. Electronic address eee, European Association for the Study of the L. EASL clinical practice guidelines: management of hepatocellular carcinoma. *J Hepatol*. 2018;69(1):182–236. doi:10.1016/j.jhep.2018.03.019.
3. Bruix J, Reig M, Sherman M. Evidence-based diagnosis, staging, and treatment of patients with hepatocellular carcinoma. *Gastroenterology*. 2016;150(4):835–853. doi:10.1053/j.gastro.2015.12.041
4. Reig M, Forner A, Rimola J, et al. BCLC strategy for prognosis prediction and treatment recommendation: the 2022 update. *J Hepatol*. 2022;76(3):681–693. doi:10.1016/j.jhep.2021.11.018
5. Llovet JM, Kelley RK, Villanueva A, et al. Hepatocellular carcinoma. *Nat Rev Dis Primers*. 2021;7(1):6. doi:10.1038/s41572-020-00240-3
6. Rimola J, Diaz-Gonzalez A, Darnell A, et al. Complete response under sorafenib in patients with hepatocellular carcinoma: relationship with dermatologic adverse events. *Hepatology*. 2018;67(2):612–622. doi:10.1002/hep.29515
7. Liu J, Boonkaew B, Arora J, et al. Comparison of sorafenib-loaded poly (lactic/glycolic) acid and DPPC liposome nanoparticles in the in vitro treatment of renal cell carcinoma. *J Pharm Sci*. 2015;104(3):1187–1196. doi:10.1002/jps.24318
8. Kim DH, Kim MD, Choi CW, et al. Antitumor activity of sorafenib-incorporated nanoparticles of dextran/poly(dl-lactide-co-glycolide) block copolymer. *Nanoscale Res Lett*. 2012;7(1):91. doi:10.1186/1556-276X-7-91
9. Mieszawska AJ, Kim Y, Gianella A, et al. Synthesis of polymer-lipid nanoparticles for image-guided delivery of dual modality therapy. *Bioconjug Chem*. 2013;24(9):1429–1434. doi:10.1021/bc400166j

10. Shen J, Sun H, Meng Q, et al. Simultaneous inhibition of tumor growth and angiogenesis for resistant hepatocellular carcinoma by co-delivery of sorafenib and survivin small hairpin RNA. *Mol Pharm*. 2014;11(10):3342–3351. doi:10.1021/mp4006408
11. Guan Q, Guo R, Huang S, et al. Mesoporous polydopamine carrying sorafenib and SPIO nanoparticles for MRI-guided ferroptosis cancer therapy. *J Controlled Release*. 2020;320:392–403. doi:10.1016/j.jconrel.2020.01.048
12. Wang CF, Makila EM, Kaasalainen MH, et al. Copper-free azide-alkyne cycloaddition of targeting peptides to porous silicon nanoparticles for intracellular drug uptake. *Biomaterials*. 2014;35(4):1257–1266. doi:10.1016/j.biomaterials.2013.10.065
13. Paşcalău V, Tertis M, Pall E, et al. Bovine serum albumin gel/polyelectrolyte complex of hyaluronic acid and chitosan based microcarriers for Sorafenib targeted delivery. *J Appl Polym Sci*. 2020;137(34):49002. doi:10.1002/app.49002
14. Chen J, Sheu AY, Li W, et al. Poly(lactide-co-glycolide) microspheres for MRI-monitored transcatheter delivery of sorafenib to liver tumors. *J Controlled Release*. 2014;184:10–17. doi:10.1016/j.jconrel.2014.04.008
15. Thapa RK, Choi JY, Poudel BK, et al. Multilayer-coated liquid crystalline nanoparticles for effective sorafenib delivery to hepatocellular carcinoma. *ACS Appl Mater Interfaces*. 2015;7(36):20360–20368. doi:10.1021/acsami.5b06203
16. Zhang H, Zhang FM, Yan SJ. Preparation, in vitro release, and pharmacokinetics in rabbits of lyophilized injection of sorafenib solid lipid nanoparticles. *Int j Nanomed*. 2012;7:2901–2910. doi:10.2147/IJN.S32415
17. Zhang Z, Niu B, Chen J, et al. The use of lipid-coated nanodiamond to improve bioavailability and efficacy of sorafenib in resisting metastasis of gastric cancer. *Biomaterials*. 2014;35(15):4565–4572. doi:10.1016/j.biomaterials.2014.02.024
18. Grillone A, Riva ER, Mondini A, et al. Active targeting of sorafenib: preparation, characterization, and in vitro testing of drug-loaded magnetic solid lipid nanoparticles. *Adv Healthc Mater*. 2015;4(11):1681–1690. doi:10.1002/adhm.201500235
19. Benizri S, Ferey L, Alies B, et al. Nucleoside-lipid-based nanocarriers for sorafenib delivery. *Nanoscale Res Lett*. 2018;13(1):17. doi:10.1186/s11671-017-2420-2
20. Bondi ML, Scala A, Sortino G, et al. Nanoassemblies based on supramolecular complexes of nonionic amphiphilic cyclodextrin and sorafenib as effective weapons to kill human HCC cells. *Biomacromolecules*. 2015;16(12):3784–3791. doi:10.1021/acs.biomac.5b01082
21. Jeevanandam J, Chan YS. Chapter 15 - In vitro and in vivo toxicity of metal nanoparticles and their drug delivery applications. In: Egbuna C, Găman M-A, Jeevanandam J, editors. *Applications of Nanotechnology in Drug Discovery and Delivery*. Elsevier; 2022:367–421.
22. Hosseinpour S, Walsh LJ, Xu C. Biomedical application of mesoporous silica nanoparticles as delivery systems: a biological safety perspective. 10.1039/D0TB01868F. *J Mat Chem B*. 2020;8(43):9863–9876. doi:10.1039/D0TB01868F
23. Wang Y, Bi K, Shu J, Liu X, Xu J, Deng G. Ultrasound-controlled DOX-SiO2 nanocomposites enhance the antitumour efficacy and attenuate the toxicity of doxorubicin. 10.1039/C8NR08497A. *Nanoscale*. 2019;11(10):4210–4218. doi:10.1039/C8NR08497A
24. Cotton GC, Lagesse NR, Parke LS, Meledandri CJ. 3.04 - antibacterial nanoparticles. In: Andrews DL, Lipson RH, Nann T, editors. *Comprehensive Nanoscience and Nanotechnology*. Second ed. Academic Press; 2019:65–82.
25. Hassan HFH, Mansour AM, Abo-Youssef AMH, Elsadek BEM, Messiha BAS. Zinc oxide nanoparticles as a novel anticancer approach; in vitro and in vivo evidence. *Clin. Exp. Pharmacol. Physiol.* 2017;44(2):235–243. doi:10.1111/1440-1681.12681
26. Fan P, Yang C, Wang L, et al. ZnO nanoparticles stimulate oxidative stress to induce apoptosis of B16F10 melanoma cells: in vitro and in vivo studies. *Biomed. Phys. Eng. Express*. 2021;7(6):065014. doi:10.1088/2057-1976/ac251f
27. de Melo Santana B, Pieretti JC, Gomes RN, Cerchiaro G, Seabra AB. Cytotoxicity towards breast cancer cells of pluronic F-127/Hyaluronic acid hydrogel containing nitric oxide donor and silica nanoparticles loaded with cisplatin. *Pharmaceutics*. 2022;14(12):2837. doi:10.3390/pharmaceutics14122837
28. Pieretti JC, Freire BM, Armentano GM, et al. Chronic exposure to nitric oxide sensitizes prostate cancer cells and improved ZnO/CisPt NPs cytotoxicity and selectivity. *Int J Pharm*. 2023;640:122998. doi:10.1016/j.ijpharm.2023.122998
29. Rodríguez-Hernández MA, Chapresto-Garzón R, Cadenas M, et al. Differential effectiveness of tyrosine kinase inhibitors in 2D/3D culture according to cell differentiation, p53 status and mitochondrial respiration in liver cancer cells. *Cell Death Dis*. 2020;11(5):339. doi:10.1038/s41419-020-2558-1
30. Bai T, Lei P, Zhou H, et al. Sigma-1 receptor protects against ferroptosis in hepatocellular carcinoma cells. *J Cell & Mol Med*. 2019;23(11):7349–7359. doi:10.1111/jcmm.14594
31. Lin CY, Chang TW, Hsieh WH, et al. Simultaneous induction of apoptosis and necroptosis by Tanshinone IIA in human hepatocellular carcinoma HepG2 cells. *Cell Death Discovery*. 2016;2(1):16065. doi:10.1038/cddiscovery.2016.65
32. Schrand AM, Schlager JJ, Dai L, Hussain SM. Preparation of cells for assessing ultrastructural localization of nanoparticles with transmission electron microscopy. *Nat Protoc*. 2010;5(4):744–757. doi:10.1038/nprot.2010.2
33. Wood LA, Larocque G, Clarke NI, Sarkar S, Royle SJ. New tools for "hot-wiring" clathrin-mediated endocytosis with temporal and spatial precision. *J Cell Biol*. 2017;216(12):4351–4365. doi:10.1083/jcb.201702188
34. Rodríguez-Hernández MA, de la Cruz-Ojeda P, Gallego P, et al. Dose-dependent regulation of mitochondrial function and cell death pathway by sorafenib in liver cancer cells. *Biochem. Pharmacol.* 2020;176:113902. doi:10.1016/j.bcp.2020.113902
35. Quy DV, Hieu NM, Tra PT, et al. Synthesis of silica-coated magnetic nanoparticles and application in the detection of pathogenic viruses. *J Nanomater*. 2013;2013(1):603940. doi:10.1155/2013/603940
36. Deepika D, PonnanEttiyappan J. Synthesis and characterization of microporous hollow core-shell silica nanoparticles (HCSNs) of tunable thickness for controlled release of doxorubicin. *J Nanopart Res*. 2018;20(7):187. doi:10.1007/s11051-018-4287-2
37. Nagaraju G, Prashanth SA, Shastri M, Yathish KV, Anupama C, Rangappa DJ. Electrochemical heavy metal detection, photocatalytic, photoluminescence, biodiesel production and antibacterial activities of Ag–ZnO nanomaterial. *Mater Res Bull*. 2017;94:54–63. doi:10.1016/j.materresbull.2017.05.043
38. Muhammad W, Ullah N, Haroon M, Abbasi BH. Optical, morphological and biological analysis of zinc oxide nanoparticles (ZnO NPs) using Papaver somniferum L. 10.1039/C9RA04424H. *RSC Adv*. 2019;9(51):29541–29548. doi:10.1039/C9RA04424H
39. Chou LYT, Ming K, Chan WCW. Strategies for the intracellular delivery of nanoparticles. 10.1039/C0CS00003E. *Chem. Soc. Rev.* 2011;40(1):233–245. doi:10.1039/C0CS00003E
40. Mahmoudi M, Tachibana A, Goldstone AB, et al. Novel MRI contrast agent from magnetotactic bacteria enables in vivo tracking of iPSC-derived cardiomyocytes. *Sci Rep*. 2016;6(1):26960. doi:10.1038/srep26960
41. Verma A, Stellacci F. Effect of surface properties on nanoparticle–cell interactions. *Small*. 2010;6(1):12–21. doi:10.1002/smll.200901158

42. Cochilla AJ, Angleson JK, Betz WJ. Monitoring secretory membrane with FM1-43 fluorescence. *Ann Rev Neurosci*. 1999;22(1):1–10. doi:10.1146/annurev.neuro.22.1.1
43. Galluzzi L, Kroemer G. Necroptosis: a specialized pathway of programmed necrosis. *Cell*. 2008;135(7):1161–1163. doi:10.1016/j.cell.2008.12.004
44. Galluzzi L, Kepp O, Chan FK-M, Kroemer G. Necroptosis: mechanisms and relevance to disease. *Annual Review of Pathology: Mechanisms of Disease*. 2017;12(12):2017):103–130. doi:10.1146/annurev-pathol-052016-100247
45. Villanueva A. Hepatocellular Carcinoma. *N Engl J Med*. 2019;380(15):1450–1462. doi:10.1056/NEJMra1713263
46. Sukhanova A, Bozrova S, Sokolov P, Berestovoy M, Karaulov A, Nabiev I. Dependence of nanoparticle toxicity on their physical and chemical properties. *Nanoscale Res Lett*. 2018;13(1):44. doi:10.1186/s11671-018-2457-x
47. Nabil A, Elshemy MM, Asem M, et al. Zinc Oxide nanoparticle synergizes sorafenib anticancer efficacy with minimizing its cytotoxicity. *Oxid Med Cell Longev*. 2020;2020:1362104. doi:10.1155/2020/1362104
48. Elkin SR, Lakoduk AM, Schmid SL. Endocytic pathways and endosomal trafficking: a primer. *Wien Med Wochenschr*. 2016;166(7–8):196–204. doi:10.1007/s10354-016-0432-7
49. Sahu D, Kannan GM, Tailang M, Vijayaraghavan R. In vitro cytotoxicity of nanoparticles: a comparison between particle size and cell type. *J Nanoscience*. 2016;2016:4023852. doi:10.1155/2016/4023852
50. Yin X, Li Z, Lyu C, et al. Induced effect of zinc oxide nanoparticles on human acute myeloid leukemia cell apoptosis by regulating mitochondrial division. *IUBMB Life*. 2022;74(6):519–531. doi:10.1002/iub.2615
51. Mingard C, Paech F, Bouitbir J, Krahenbuhl S. Mechanisms of toxicity associated with six tyrosine kinase inhibitors in human hepatocyte cell lines. *J Appl Toxicol*. 2018;38(3):418–431. doi:10.1002/jat.3551